ISSN 1063-7834, Physics of the Solid State, 2019, Vol. 61, No. 8, pp. 1502–1508. © Pleiades Publishing, Ltd., 2019.
Russian Text © The Author(s), 2019, published in Fizika Tverdogo Tela, 2019, Vol. 61, No. 8, pp. 1550–1556.

GRAPHENES

Surface Plasmon Polaritons in a Graphene–Semiconductor–Graphene Thin Film

A. S. Abramov[a], D. A. Evseev[a], and D. I. Sementsov[a, *]

[a] *Ulyanovsk State University, Ulyanovsk, 432017 Russia*

**e-mail: sementsovdi@mail.ru*

Received December 27, 2018; revised December 27, 2018; accepted April 16, 2019

Abstract—Dispersion properties of surface plasmon polaritons in a semiconductor film with graphene plates in the far-IR range and the possibility of controlling propagation modes due to the change in the chemical potential on one or both plates have been investigated. Dispersion relations for the TE- and TM-polarized waves have been obtained and analyzed, and distributions of the wave field and energy fluxes over the structure have been constructed. Spectral ranges where the surface-wave group velocity is negative are found.

Keywords: semiconductor film, graphene layers, chemical potential, plasmon polaritons, dispersion properties

DOI: 10.1134/S106378341908002X

1. INTRODUCTION

Properties of surface plasmon polaritons (SPPs) are known to be basically determined by the character of dispersion of the material parameters of adjacent media. In metal–dielectric guiding structures, the existence of SPPs is caused by the presence of a wide frequency region, in which the metal permittivity is negative. The behavior of SPPs in these structures and the possibility of their practical application were considered in detail in [1–7]. However, the use of a metal as the guiding surface inevitably leads to fast damping and small free paths of polaritons. In this context, structures based on semiconductor materials, in which surface waves can also exist below the plasma frequency and their parameters can be controlled, may be of great interest [8–11].

Currently, graphene and various related structures are considered as promising materials for photonics. The physical properties of graphene structures may differ significantly from those of structures based on other materials because of the specific features of graphene conductivity dispersion [12–18]. The guiding properties of graphene structures, which can retain localized plasmon modes in a wide frequency range (from THz to optical region) both on a graphene monolayer and on two or more its layers separated by insulator layers, are of great importance in practice [19–22].

In this paper, we report the results of studying the conditions of existence of SPPs in a thin semiconductor film with graphene layers deposited at both sides and analyzing the possibility of control of their dispersion characteristics by changing the graphene chemical potential (CP), as well as showing the possibility of significant slowing-down of the waves propagating in the structure and achievement of negative values of their group velocity.

2. MATERIAL PARAMETERS OF THE STRUCTURE

Propagation of SPPs will be considered in the structure consisting of a thin, lightly doped semiconductor film with thickness d with a graphene layer deposited on both surfaces (or one surface). The film with graphene layers is between two media with frequency-independent permittivities ε_1 and ε_3. The semiconductor permittivity within the Drude–Lorentz approximation can be presented in the form

$$\varepsilon_2(\omega) = \varepsilon_1\left(1 - \frac{\omega_p^2}{\omega(\omega + i\gamma)}\right), \qquad (1)$$

where ε_1 is the lattice contribution, ω_p is the plasma frequency, and γ is the relaxation rate [16]. The permeabilities of all media are assumed to be unity.

The frequency dependence of the real and imaginary components of the surface conductivity of doped graphene $\sigma = \sigma' + i\sigma''$ within the Kubo model is determined by the relations [15, 17]

$$\frac{\sigma'}{\sigma_0} = \frac{1}{2} + \frac{1}{\pi}\arctan\left(\frac{\hbar\omega - 2\mu}{2k_bT}\right),$$

$$\frac{\sigma''}{\sigma_0} = \frac{1}{2\pi}\left[\frac{16k_BT}{\hbar\omega}\ln\left(2\cosh\left(\frac{\mu}{2k_BT}\right)\right)\right. \qquad (2)$$

$$- \ln\left(\frac{(\hbar\omega + 2\mu)^2}{(\hbar\omega - 2\mu)^2 + (2k_B T)^2}\right)\Bigg],$$

where $\sigma_0 = e^2/4\hbar$ is the fundamental (static) graphene conductivity, e is the elementary charge, $\hbar$ is Planck's constant, k_B is the Boltzmann constant, T is temperature, and $\mu = \hbar v_F \sqrt{\pi n_0}$ is the CP (n_0 is the charge-carrier concentration and v_F is the Fermi velocity in graphene). Figure 1 shows the frequency dependences of the real and imaginary components of the graphene surface conductivity plotted in accordance with expressions (2) for temperature $T = 300$ K and CP values $\mu = 0$, 0.1, and 0.3 eV (curves *1*–*3*, respectively). The CP value in an experiment can be efficiently controlled by an external electric field and temperature [18].

3. WAVE FIELDS AND DISPERSION RELATION

Let us assume that linearly polarized localized waves of two types—TM and TE with the field components (E_x, H_y, E_z) and (H_x, E_y, H_z), respectively—can propagate in the structure under study along the *OX* axis oriented parallel to the interface. Each of these components depends on time and coordinates as follows:

$$F_a(x, z, t) = F_a(z)\exp[i(\omega t - \beta x)], \qquad (3)$$

where $F_a(z)$ are the profile functions, β is the propagation constant, and ω is frequency. The equations for the wave-field profile functions in each medium (j = 1, 2, 3) have the form

$$\frac{\partial^2 F_y}{\partial z^2} - q_j^2 F_y = 0. \qquad (4)$$

Here, $F_y = H_y$ for the TM wave, $F_y = E_y$ for the TE wave, and transverse wave-vector components are $q_j = \sqrt{\beta^2 - k_0^2 \varepsilon_j}$ ($k_0 = \omega/c$ and c is the speed of light in vacuum). The q_j values characterize the wave type and penetration depth of the surface-wave (SW) field into the substrate and coating. The necessary conditions of existence of the waveguide mode in the structure are inequalities $\mathrm{Re}\, q_j^2 > 0$, which ensure exponential falloff of the wave-field amplitude while moving away from the interface. The inequalities $\beta' > 0$ and $\beta'' > 0$ must also be satisfied; the former indicates the positivity of the wave phase velocity in the structure, while the latter indicates the absence of amplification. The existence of the SW in the structure is determined by the condition $\mathrm{Re}\, q_2^2 = \mathrm{Re}(\beta^2 - k_0^2\varepsilon_2) > 0$; when this inequality is invalid, waveguide modes may propagate in the structure.

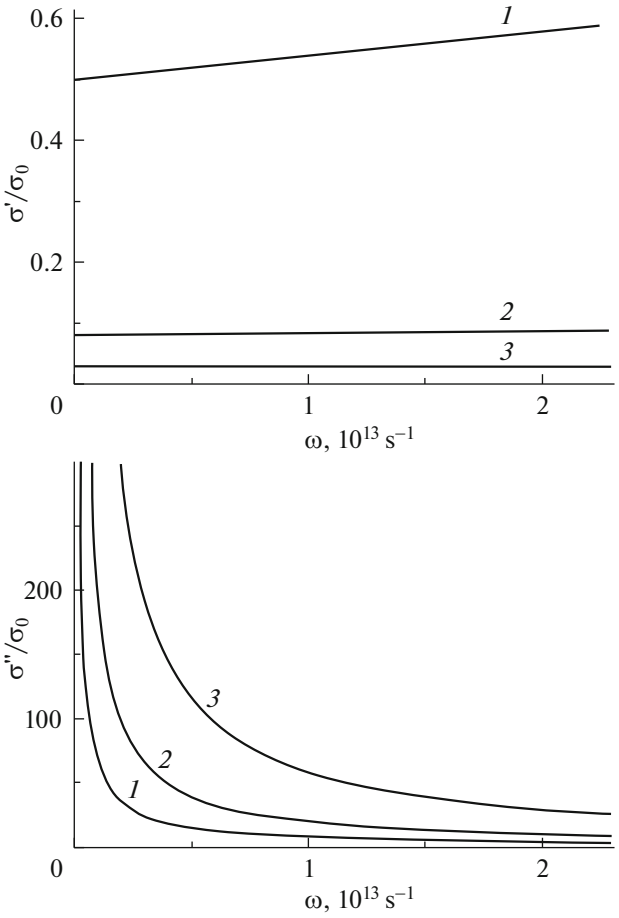

Fig. 1. Frequency dependences of the real and imaginary parts of the graphene surface conductivity at $\mu_{1,3} = 0$, 0.1, and 0.3 eV (curves *1*–*3*, respectively).

The solution to Eq. (4) for the surface TM wave can be written as

$$F_y(z) = \begin{cases} A_1 \exp(q_1 z), & z < 0, \\ A_2 \cosh(q_2 z) + A_3 \sinh(q_2 z), & 0 < z < d, \\ A_1 \exp(-q_3 z), & z > d. \end{cases} \qquad (5)$$

To determine coefficients A_j entering (5) and find the dispersion relation, we use the boundary conditions for tangential components of the electric and magnetic fields at $z = 0$, d:

$$\begin{gathered} E_{1,3x} = E_{2x}, \\ H_{1,3y} - H_{2y} = \pm(4\pi/c)\sigma_{1,3}E_{1,3x}\ (\mathrm{TM}), \\ E_{1,3y} = E_{2y}, \\ H_{1,3x} - H_{2x} = \mp(4\pi/c)\sigma_{1,3}E_{1,3y}\ (\mathrm{TE}). \end{gathered} \qquad (6)$$

To solve these equations, one should take into account the following relationships between the wave-field

components for the TM and TE waves, respectively:

$$E_x = (ik_0\varepsilon_j)^{-1}(\partial H_y/\partial z), \quad E_z = (\beta/k_0\varepsilon_j)H_y \text{ (TM)},$$
$$H_x = (ik_0)^{-1}(dE_y/dz), \quad H_z = (\beta/k_0)E_y \text{ (TE)}. \tag{7}$$

With allowance for (5)–(7), we find the following dispersion relations for the corresponding wave types:

$$\exp(2q_2d) = \frac{1-\dfrac{\varepsilon_1 q_2}{\varepsilon_2 q_1} - i\dfrac{4\pi\sigma_1 q_2}{\varepsilon_2 c k_0}}{1+\dfrac{\varepsilon_1 q_2}{\varepsilon_2 q_1} + i\dfrac{4\pi\sigma_1 q_2}{\varepsilon_2 c k_0}} \times \frac{1-\dfrac{\varepsilon_3 q_2}{\varepsilon_2 q_1} - i\dfrac{4\pi\sigma_3 q_2}{\varepsilon_2 c k_0}}{1+\dfrac{\varepsilon_3 q_2}{\varepsilon_2 q_3} + i\dfrac{4\pi\sigma_1 q_2}{\varepsilon_2 c k_0}} \text{ (TM)},$$
$$\exp(2q_2d) = \frac{1-\dfrac{q_2}{q_1} - i\dfrac{4\pi\sigma_1 k_0}{c q_2}}{1+\dfrac{q_2}{q_1} + i\dfrac{4\pi\sigma_1 k_0}{c q_2}} \frac{1-\dfrac{q_2}{q_3} - i\dfrac{4\pi\sigma_3 k_0}{c q_2}}{1+\dfrac{q_2}{q_3} + i\dfrac{4\pi\sigma_3 k_0}{c q_2}} \text{ (TE)}. \tag{8}$$

Taking into account the complexity of the parameters entering these equations, the latter determine the relationship between the real and imaginary components of the wave number $\beta = \beta' - i\beta''$ and the electromagnetic-wave frequency. Equations (8) are written for the case of different conductivities of the graphene layers. In the absence of graphene layers, $\sigma_1 = \sigma_3 = 0$, and Eqs. (8) are reduced to the standard dispersion relations for SWs in a dielectric waveguide [4, 19]. For symmetric plates ($\varepsilon_1 = \varepsilon_3 = \varepsilon$ and $\sigma_1 = \sigma_3 = \sigma$), these equations take the simpler form:

$$\exp(q_2d) = \left(1-\frac{\varepsilon q_2}{\varepsilon_2 q} - i\frac{4\pi\sigma q_2}{\varepsilon_2 c k_0}\right) \times \left(1+\frac{\varepsilon q_2}{\varepsilon_2 q} + i\frac{4\pi\sigma q_2}{\varepsilon_2 c k_0}\right)^{-1} \text{ (TM)},$$
$$\exp(q_2d) = \left(1-\frac{q_2}{q} - i\frac{4\pi\sigma k_0}{c q_2}\right) \times \left(1+\frac{q_2}{q} + i\frac{4\pi\sigma k_0}{c q_2}\right)^{-1} \text{ (TE)}, \tag{9}$$

where $q_1 = q_3 = q$. The dispersion relation for TE was written taking into account that the permeabilities of all media equal unity.

4. NUMERICAL ANALYSIS

The results of the numerical analysis of SW propagation modes in the structure under consideration are given below. The dielectric response of the semiconductor layer is determined by expression (1), in which the static permittivity is $\varepsilon_l = 10.9$, the plasma frequency is $\omega_p = 2.07 \times 10^{13}$ s^{-1}, and the carrier relaxation rate is $\gamma = 0.05\omega_p$. Hereinafter, we assume that the film with the graphene layers is in vacuum (therefore, $\varepsilon_1 = \varepsilon_3 = 1$).

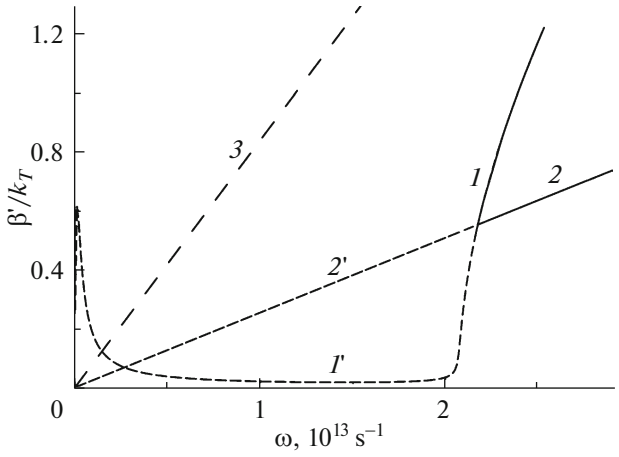

Fig. 2. Frequency dependences of the propagation constant for TE waves at $d = 0$ nm; dotted curves *1'* and *2'* correspond to the semiconductor photon line $\beta = k_0\sqrt{\varepsilon_2(\omega)}$ and the cutoff line $\beta = k_0\sqrt{\varepsilon}$, respectively.

Figure 2 shows the dispersion relations, which are the solution to Eq. (7) for the TE wave at the waveguiding-layer thickness $d = 10$ nm. The propagation constant β' is normalized to the quantity $k_T = k_B T/hc$, the value of which is $k_T = 1314.24$ cm^{-1} for the operating temperature $T = 300$ K. Dotted curves *1'* and *2'* correspond to the dependences $\beta = k_0\sqrt{\varepsilon_2(\omega)}$ and $\beta = k_0\sqrt{\varepsilon}$, which have the meaning of a photon line in unbounded semiconductor and a cutoff line of a planar waveguide. Above the plasma frequency, these curves limit the domain of existence of the waveguide modes of this waveguide. Below the plasma frequency in the structure, there are no solutions corresponding to the waveguide and surface modes. The dashed line corresponds to the dependence $\beta = k_0\sqrt{\varepsilon_l}$, which is a photon line for insulator with permittivity ε_l. Thus, it can be seen in the figure that the solutions to the dispersion equations for the TE waves are not implemented in the region of negative semiconductor permittivity. The reason is that the only component of the wave electric field (in the case of TE wave) makes electrons to oscillate across the wave-propagation direction. Here, the excitation of plasmons—quanta of longitudinal oscillations of the electron plasma (i.e., directed along the electromagnetic-wave propagation direction)—is hindered.

In the domain of existence of the waveguide modes ($\omega > \omega_p$), there are two different solutions to these equations, one of which practically coincides with cutoff line *2* and is a zero mode of the planar waveguide. The second solution coincides with the dependence

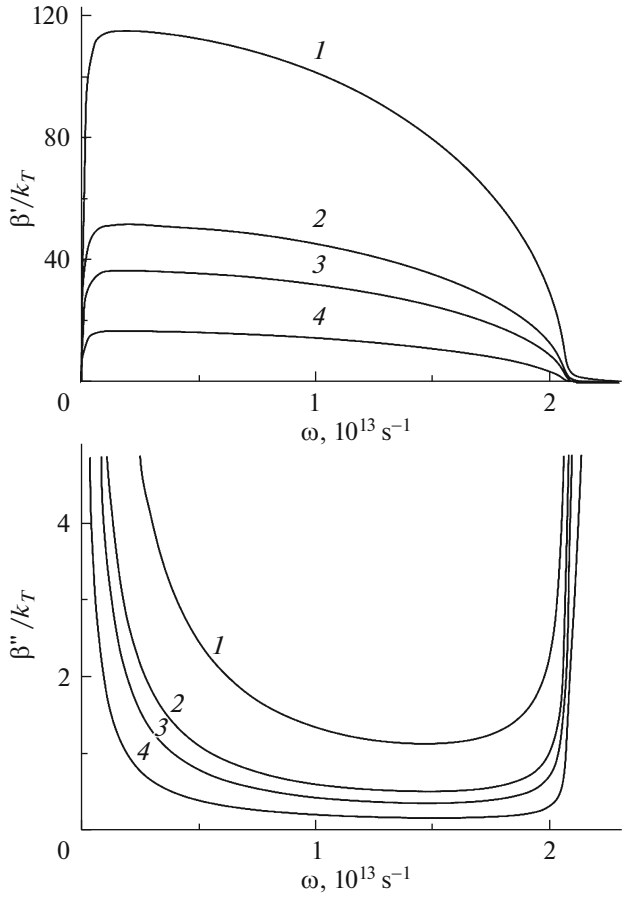

Fig. 3. Frequency dependences of the real and imaginary parts of the propagation constant of the surface TM wave at $\mu_{1,3} = 0.3$ eV and semiconductor film thickness $d = 10$, 50, 100, and 500 nm (curves *1*–*4*, respectively).

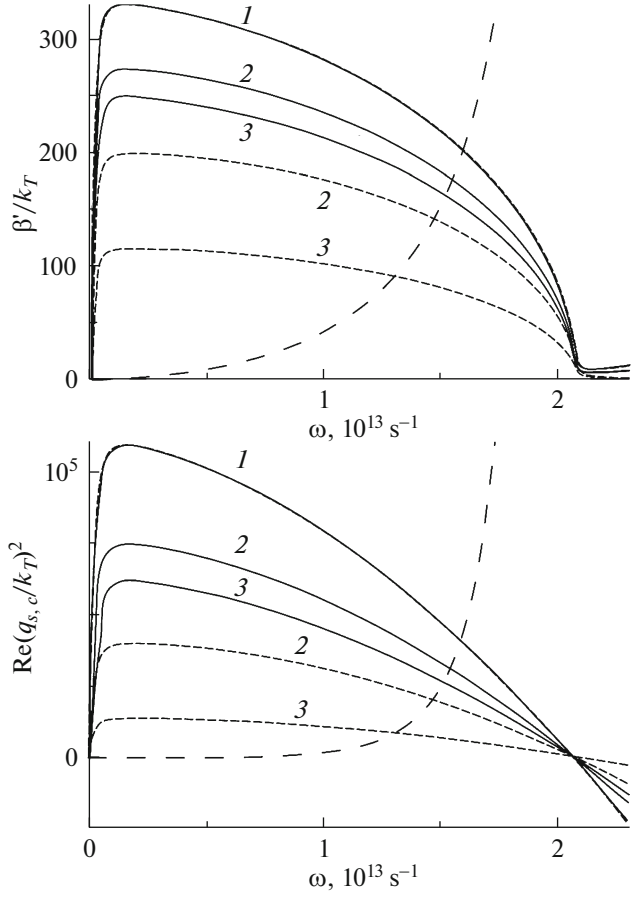

Fig. 4. Frequency dependences of the propagation constant and squared transverse wave-vector component at $\mu_{1,3} = 0$, 0.1, and 0.3 eV (solid curves *1*–*3*) and $\mu_1 = 0$ eV and $\mu_3 = 0$, 0.1, and 0.3 eV (dotted curves *1*–*3*); the dashed curve corresponds to the case without graphene.

$\beta = k_0\sqrt{\varepsilon_2(\omega)}$ (curve *1*) and is an analog of the solution obtained in [20] for a dielectric planar waveguide with graphene plates. A distinctive feature of this wave is fulfillment of the condition $\mathrm{Re}q_2^2 = 0$ for any frequency in this range. With an increase in the semiconductor layer thickness, no surface modes are implemented in the frequency region below the plasma frequency.

Let us now consider the propagation of the TM-polarized wave in the structure. Figure 3 shows the dependences of the real and imaginary components of the propagation constant of the surface TM wave on frequency, which are solutions to Eq. (9) at the graphene-layer CP $\mu_1 = \mu_3 = 0.3$ eV and film thicknesses $d = 10$, 50, 100, and 500 nm (curves *1*–*4*). The solutions exist in the region of negativity of $\varepsilon_2'(\omega)$, which is the condition of existence of the wave localized at the interface. In this region, the propagation constant achieves a maximum at frequency ω_{cr} determined by the equality $d\beta'/d\omega = 0$. The range of values for each component of the propagation constant in the entire frequency range significantly decreases with an increase in the film thickness. Note that the parameter $\beta'' \sim 1/\gamma$ (γ is the surface polariton free path) is smaller than $\beta' \sim 1/\lambda$ (λ is the wavelength) by two orders of magnitude in a rather wide frequency range below the plasma frequency $\omega_p = 2.07 \times 10^{13}$ s^{-1}. At frequencies $\omega > \omega_p$, the wave propagation length sharply decreases, and β' tends to the cutoff line.

Important characteristics of the wave field in the structure are transverse wave-vector components $q_{1,3}$. The existence of the SW in a certain frequency region is indicated by the positivity of parameter $\mathrm{Re}(q_{1,3})^2$. At the same time, the quantity $\delta_{1,3} = 1/q'_{1,3}$ determines the penetration depth of the SW wave field into each medium adjacent to the waveguiding layer. The frequency dependences of the real components of the propagation constant and squared transverse wave-vector component of the surface TM wave for two- and one-sided CP variations (solid and dotted curves) are shown in Fig. 4 for the film thickness $d = 10$ nm.

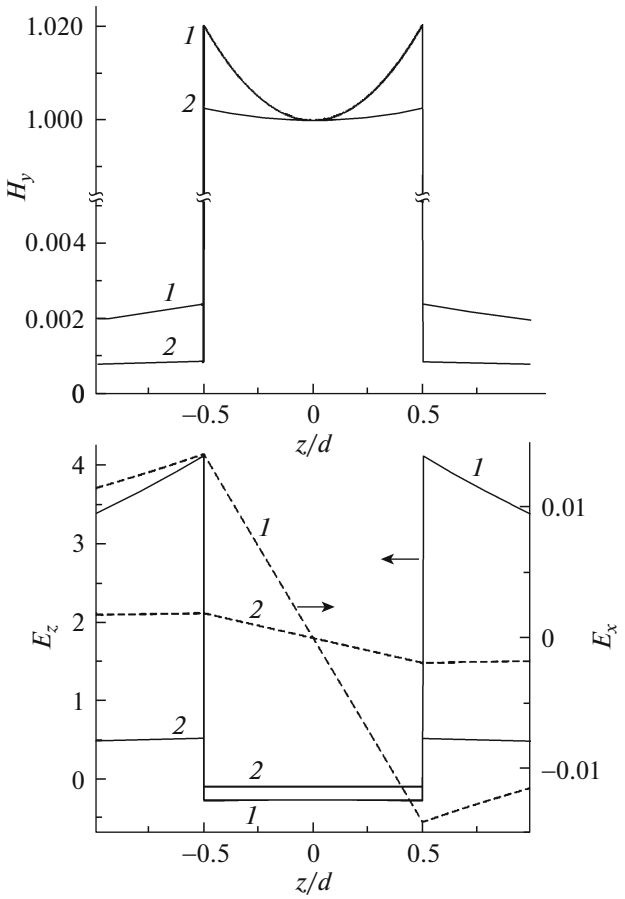

Fig. 5. Field distributions H_y and E_z of the TM wave over the structure cross section at $\mu_{1,3} = 0$ and 0.3 eV (curves *1* and *2*, respectively), $d = 10$ nm, and $\omega = 0.7 \times 10^{13}$ s^{-1}.

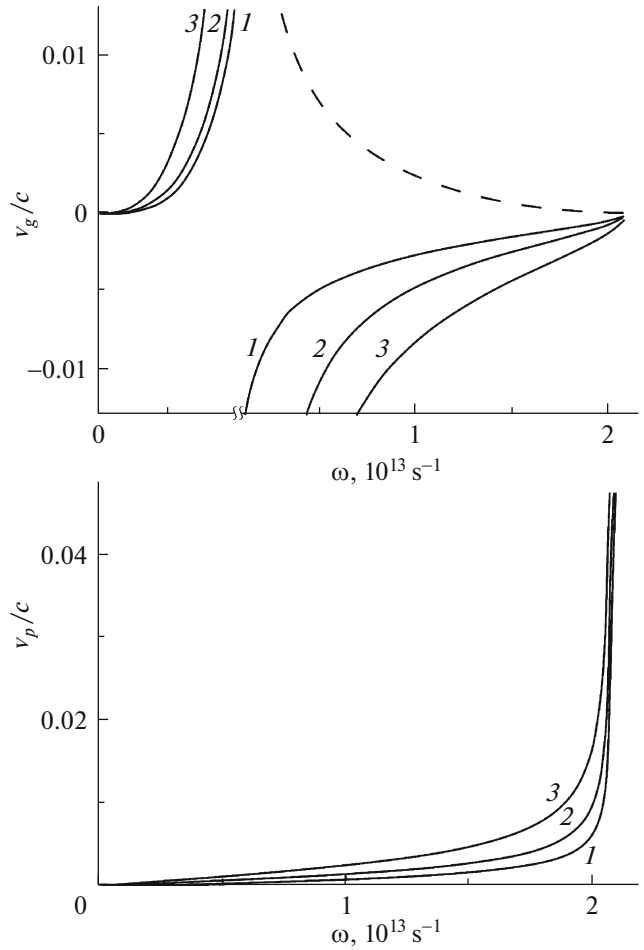

Fig. 6. Frequency dependences of the group and phase velocities of the TM wave at $\mu_{1,3} = 0$, 0.1, and 0.3 eV (curves *1–3*, respectively); the dashed curve corresponds to the case without graphene.

In the first case, $\mu_1 = \mu_3$; in the second case, $\mu_1 = 0$; and $\mu_3 = 0$, 0.1, and 0.3 eV in both cases (curves *1–3*, respectively). The dashed line corresponds to the dispersion of the structure without graphene layers.

It can be seen in the presented dependences that, below the plasma frequency, the function $\beta'(\omega)$ is monotonically decreasing in the most part of the domain of existence of the SW, which is indicative of the negativity of the SW group velocity (in the absence of graphene, the group velocity remains positive). The range of values of the parameters under consideration decreases in the entire frequency range with an increase in the CP. It can also be seen that the minimum SW location depth in each medium is observed in the region of maximum propagation constants, whereas the maximum location depth is near the plasmon resonance. Above the plasma frequency, the imaginary part of the propagation constant sharply increases, and the quantity $\mathrm{Re}(q_{1,3})^2$ becomes negative. The reason is that the semiconductor permittivity becomes positive in this region, and the SW is transformed into a radiative wave. The propagation length of this wave is small, and the most part of its energy is emitted to the coating layers and partially absorbed by free carriers in semiconductor and graphene. The criterion of SW transformation into a bulk wave can be assumed to be validity of the inequalities $\delta_d \gg \lambda/\sqrt{\varepsilon_d}$, where $\lambda = 2\pi c/\omega$ is the wavelength in vacuum. The waveguide modes cannot exist in the structure as well, because the chosen waveguiding-layer thicknesses are much smaller than the wavelength in the semiconductor ($d \ll \lambda/\sqrt{\varepsilon_2}$).

Figure 5 shows the distributions of the magnetic and electric SW fields over the structure cross section corresponding to the frequency $\omega = 0.7 \times 10^{13}$ s^{-1}, $d =$ 10 nm, and CP values $\mu_1 = \mu_3 = 0$ and 0.3 eV (curves *1* and *2*). At symmetric CP values, the component distributions $H_y(z)$ and $E_z(z)$ are symmetric with respect to the structure, while $E_x(z)$ is antisymmetric (dotted line). The presence of the graphene layers results in the discontinuity of the magnetic field at the wave-

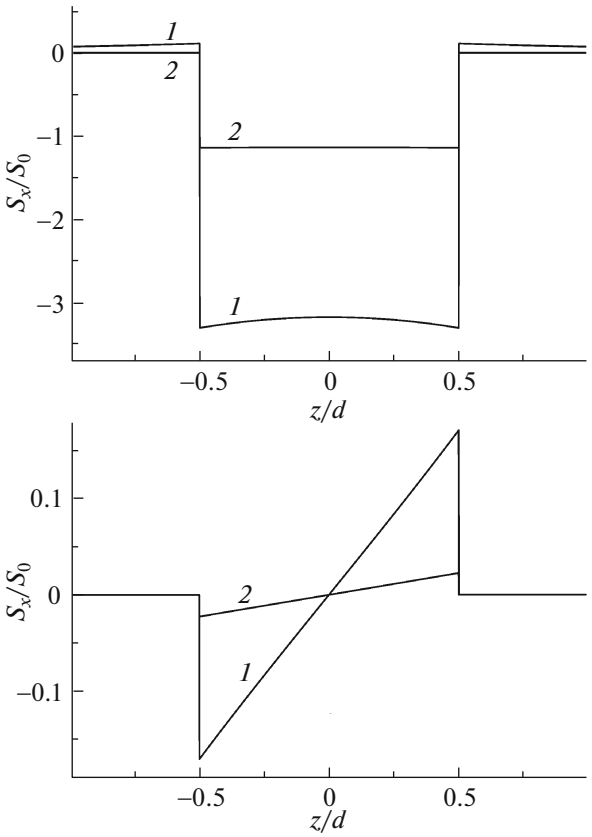

Fig. 7. Distributions of the longitudinal $\langle S_x \rangle$ and transverse $\langle S_z \rangle$ components of the energy flux density at $\mu_{1,3} = 0$ and 0.3 eV (curves *1* and *2*, respectively).

guiding-layer boundaries. At $\mu_1 \neq \mu_3$, the symmetry in the field distribution disappears. The wave-field distribution in the structure and its dispersion properties can be significantly modified by changing the CP value.

Let us now consider the frequency dependences of the characteristic SW velocities, which were plotted using the CP value of $\mu_1 = \mu_3 = 0$, 0.1, and 0.3 eV (curves *1–3*, respectively); the dashed line corresponds to the structure without graphene layers (Fig. 6), for which the group velocity $v_g = d\omega/d\beta'$ is positive in the frequency range under consideration. The SW group velocity takes positive values in the region below the critical frequency, corresponding to the maximum of the dispersion curve $\beta'(\omega)$, and negative values for frequencies $\omega > \omega_{cr}$. The group velocity is lower than the speed of light in vacuum by two or more orders of magnitude far from ω_{cr} and asymptotically increases at $\omega \to \omega_{cr}$. At $\omega \to \omega_p$, the group velocity tends to zero, i.e., there is significant slowing down of the SW. An increase in the CP leads to a rise in the magnitude of the group velocity.

A slow increase in the phase velocity $v_{ph} = \omega/\beta'$ is observed far from ω_p; as for the group velocity, v_{ph} is lower than the speed of light in vacuum by two or more orders of magnitude. This parameter sharply increases in a narrow spectral range near the plasma frequency.

The energy characteristic of the wave process with allowance for its harmonic time dependence is the Poynting vector $\langle \mathbf{S} \rangle = (c/8\pi)\mathrm{Re}(\mathbf{E} \times \mathbf{H}^*)$ determining (in the case under consideration) period-averaged SW energy flux density. The presence of the transverse and longitudinal electric-field components leads to the fact that vector $\langle \mathbf{S} \rangle$ also has the longitudinal $\langle S_x \rangle$ and transverse $\langle S_z \rangle$ components. Figure 7 shows the distributions of these parameters (normalized to $S_0 = cH_0^2/8\pi$) over the structure, obtained for $d = 10$ nm, $\omega = 0.7 \times 10^{13}$ s^{-1}, and $\mu_1 = \mu_3 = 0$ and 0.3 eV (curves *1* and *2*, respectively). The flux component $\langle S_x \rangle$ is distributed symmetrically over the structure and has a negative sign (i.e., it is directed opposite to the phase velocity), whereas the component $\langle S_z \rangle$ is distributed antisymmetrically. It can be seen that there is no transverse flux component in the central cross section of the structure; while moving away from it, the flux component $\langle S_z \rangle$ increases, thus transferring some energy to the boundaries of the structure (i.e., facilitates its localization).

5. CONCLUSIONS

Specific features of SW propagation in a semiconductor layer between two graphene layers were investigated. The dispersion relations for intrinsic TM and TE waves in the structure were obtained based on the solution of the boundary problem. Proceeding from the numerical analysis of the dispersion relations, the frequency dependences of the propagation constant and group and phase velocities, as well as the distributions of the wave fields and energy fluxes, were plotted for the frequency region below the plasma frequency. It was shown that, in the region of negative semiconductor permittivities, there are no solutions corresponding to the surface TE waves in the considered structure. For surface TM waves, the group velocity takes positive values in the region below the critical frequency corresponding to the maximum in the dispersion curve $\beta'(\omega)$ and negative values for frequencies $\omega > \omega_p$. Far from ω_{cr}, the group velocity is lower than the speed of light in vacuum by two or more orders of magnitude, i.e., the SW is significantly slowed down. The increase in the graphene-layer CP leads to a rise in the magnitude of the group velocity. The longitudinal component of the energy flux $\langle S_x \rangle$ is distributed symmetrically over the structure and has a negative sign in the region $\omega > \omega_{cr}$ (i.e., it is directed opposite to the phase velocity). The analysis showed the possibility of controlling the SW dispersion characteristics by changing the graphene-layer CP, plasma fre-

quency, and semiconductor layer thickness. Note also that SWs in the structure can be efficiently controlled using an external magnetic field, which strongly affects not only the semiconductor state but also the graphene state. However, these questions require separate consideration.

FUNDING

This study was supported by the Russian Science Foundation, project no. 17-72-10135, and the Ministry of Education and Science of the Russian Federation, project no. 3.6825/BCh.

CONFLICT OF INTEREST

The authors declare that they have no conflicts of interest.

REFERENCES

1. *Surface Polaritons*, Ed. by V. M. Agranovich and D. L. Mills (North-Holland, Amsterdam, 1982; Nauka, Moscow, 1985).
2. A. A. Semenov, S. F. Karmanenko, A. A. Melkov, A. V. Bobyl', R. A. Suris, Yu. M. Gal'perin, and T. H. Johansen, Tech. Phys. **46**, 1218 (2001).
3. S. Maier, *Plasmonics: Fundamentals and Applications* (Springer, New York, 2007).
4. V. I. Belotelov, D. A. Bykov, L. L. Doskolovich, A. N. Kalish, and A. K. Zvezdin, Phys. Solid State **51**, 1656 (2009).
5. D. Yu. Fedyanin, A. V. Arsenin, V. G. Leiman, and A. D. Gladun, Quantum Electron. **39**, 745 (2009).
6. A. S. Abramov, I. O. Zolotovskii, D. G. Sannikov, and D. I. Sementsov, Phys. Solid State **57**, 652 (2015).
7. G. W. Hanson, J. Appl. Phys. **103**, 064302 (2008).
8. N. L. Dmitruk, V. G. Litovchenko, and V. L. Strizhevskii, *Surface Polaritons in Semiconductors and Dielectrics* (Naukova Dumka, Kiev, 1989) [in Russian].
9. G. A. Martsinovsky, G. D. Shandybina, Yu. S. Dement'eva, R. V. Dyukin, S. V. Zabotnov, L. A. Golovan', and P. K. Kashkarov, Semiconductors **43**, 1298 (2009).
10. V. A. Kosobukin, Phys. Solid State **59**, 999 (2017).
11. A. S. Abramov, I. O. Zolotovskii, S. G. Moiseev, and D. I. Sementsov, Quantum Electron. **48**, 22 (2018).
12. S. V. Morozov, K. S. Novoselov, and A. K. Geim, Phys. Usp. **51**, 744 (2008).
13. A. H. Castro Neto, F. Guinea, N. M. R. Peres, K. S. Novoselov, and A. K. Geim, Rev. Mod. Phys. **81**, 109 (2009).
14. L. A. Falkovsky, Phys. Usp. **55**, 1140 (2012).
15. Yu. E. Lozovik, Phys. Usp. **55**, 1035 (2012).
16. Z. Z. Alisultanov and R. P. Meilanov, Phys. Solid State **54**, 1486 (2012).
17. D. Yu. Usachov, A. V. Fedorov, O. Yu. Vilkov, B. V. Senkovskiy, V. K. Adamchuk, B. V. Andryushechkin, and D. V. Vyalikh, Phys. Solid State **55**, 1325 (2013).
18. G. W. Hanson, J. Appl. Phys. **104**, 084314 (2008).
19. P. I. Buslaev, I. V. Iorsh, I. V. Shadrinov P. A. Belov, and Yu. S. Kivshar, JETP Lett. **97**, 535 (2013).
20. D. Smirnova, P. Buslaev, I. Iorsh, I. V. Shadrivov, P. A. Belov, and Yu. S. Kivshar, Phys. Rev. B **89**, 245414 (2014).
21. D. A. Smirnova, I. V. Iorsh, I. V. Shadrivov, and Yu. S. Kivshar, JETP Lett. **99**, 456 (2014).
22. D. A. Evseev and D. I. Sementsov, Phys. Solid State **60**, 616 (2018).

Translated by A. Sin'kov